



A global statistical study on the origin of small-scale ozone vertical structures in the lower stratosphere

K. Noguchi,^{1,2} T. Imamura,³ K.-I. Oyama,³ and G. E. Bodeker⁴

Received 27 February 2006; revised 3 July 2006; accepted 9 August 2006; published 14 December 2006.

[1] We investigated meridional and seasonal variations in small-vertical-scale (wavelengths 0.5–3 km) fluctuations of the ozone mixing ratio in the lower stratosphere using ozonesonde data covering wide longitudinal and latitudinal regions in all seasons. The generation of mixing ratio fluctuation is attributed to vertical advection and/or horizontal advection; the former was estimated from the potential temperature fluctuation and the vertical gradient of background mixing ratio, while the latter was obtained by subtracting the vertical advection component from the observed value. The results show that horizontal advection is always the major source of the mixing ratio fluctuation above the potential temperature of 700 K (~ 27 km altitude). Below 700 K, the source of the mixing ratio fluctuation depends on latitude; horizontal advection governs the mixing ratio fluctuations at high latitudes, vertical advection dominates at low latitudes, and horizontal advection is relatively dominant in winter–spring, while vertical advection is dominant in summer–autumn in the midlatitudes. These tendencies were confirmed by analyzing the correlation between the small-scale structures of the mixing ratio and the potential temperature. The synthetic distribution of the horizontal advection activity due to synoptic-scale motions calculated from assimilated meteorological data reproduced the seasonal, meridional, and altitudinal tendencies of the observed small-scale fluctuations, suggesting the major contribution of differential advection via large-scale winds.

Citation: Noguchi, K., T. Imamura, K.-I. Oyama, and G. E. Bodeker (2006), A global statistical study on the origin of small-scale ozone vertical structures in the lower stratosphere, *J. Geophys. Res.*, *111*, D23105, doi:10.1029/2006JD007232.

1. Introduction

[2] Small-scale layered structures observed in the vertical profiles of passive tracers are direct evidence of the transport of air from regions of differing background tracer abundances. Ozone is one of such passive tracer in the lower stratosphere since it has a lifetime exceeding several months [e.g., *Brasseur and Solomon*, 1986]. Figure 1 shows the seasonal variation of the meridional cross section of the zonal mean ozone mixing ratio based on satellite-based observations provided by the Upper Atmosphere Research Satellite Reference Atmosphere Project (URAP) [see *Swinbank and Ortland*, 2003], suggesting the presence of horizontal and vertical gradients of the mixing ratio. Temporal fluctuations in tracer abundances occur when air parcels are displaced across such mixing ratio gradients. In the present study, these displacements of air parcels are called advection, irrespective of whether the displacements occur irreversibly. Horizontal and vertical advectations are

defined as advection along and across isentropic surfaces, respectively. When they occur irreversibly, these types of advection contribute differently to the diffusive transport of atmospheric constituents and energy.

[3] Previous studies have suggested that horizontal diffusion coefficients range from $D_H = 10^5$ to 10^6 m² s⁻¹ in the stratosphere [e.g., *Lyjak and Yudin*, 2005], which corresponds to the time constants of $a^2/D_H = 1$ –10 years, where a is the planetary radius. Vertical diffusion coefficients have been estimated as $D_V = 0.1$ –1 m² s⁻¹ [e.g., *Fukao et al.*, 1994], corresponding to time constants of $H^2/D_V = 2$ –20 years, where $H = 8$ km is the typical scale height. Because these diffusive transports are not negligible when compared with transport by the Brewer-Dobson circulation, which has a time constant of ~ 2 years [*Holton et al.*, 1995], the process of tracer layering is one of the keys to understanding the transport of atmospheric constituents and energy in the stratosphere.

[4] The dynamical processes that cause the layered structures of the ozone mixing ratio include differential advection, i.e., the conversion of filamentary horizontal structures into layered vertical structures via large-scale horizontal winds accompanied by vertical shear. This process works even when small-scale structures are absent in the wind field [*Newman and Schoeberl*, 1995; *Orsolini et al.*, 1995; *Schoeberl and Newman*, 1995]. Horizontal filamentation of tracers is frequently caused by planetary wave breaking and polar vortex erosion [*McIntyre and Palmer*, 1983; *Juckes*

¹Faculty of Science, Nara Women's University, Nara, Japan.

²Formerly at Institute of Space and Astronautical Science, Japan Aerospace Exploration Agency, Kanagawa, Japan.

³Institute of Space and Astronautical Science, Japan Aerospace Exploration Agency, Kanagawa, Japan.

⁴National Institute of Water and Atmospheric Research, Omakau, New Zealand.

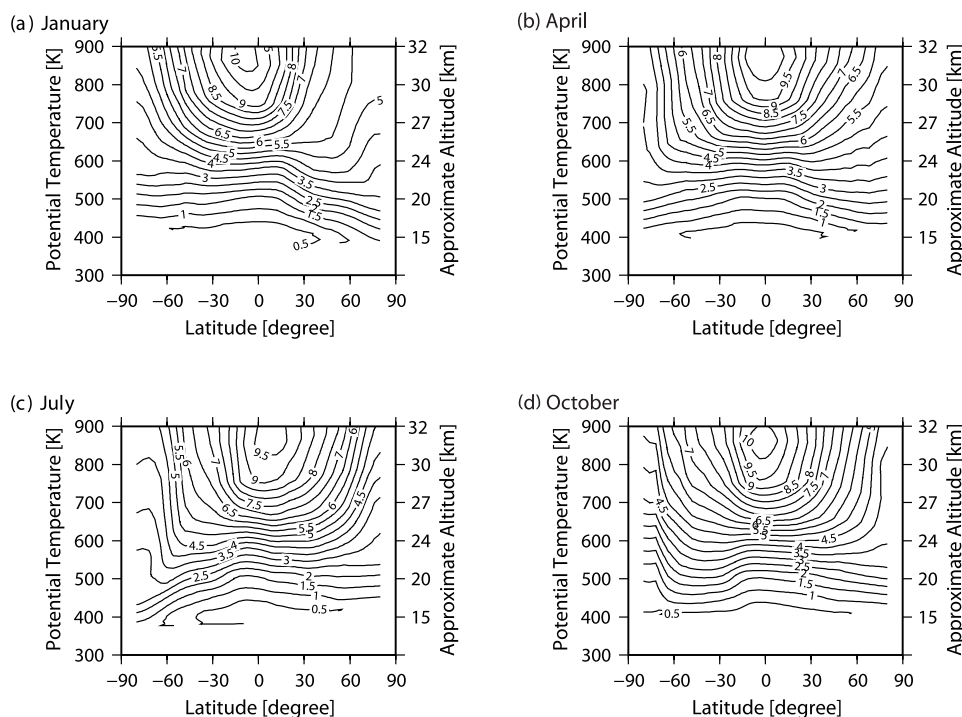


Figure 1. Meridional distribution of the ozone mixing ratio in ppmv in (a) January, (b) April, (c) July, and (d) October taken from the URAP data set. The approximate height on the right side of each plot was calculated from U.S. Standard Atmosphere (1976).

and McIntyre, 1987; Plumb *et al.*, 1994; Waugh *et al.*, 1994]. Planetary waves and their breaking also cause vertically sheared horizontal winds [Tomikawa *et al.*, 2002; Portafaix *et al.*, 2003], which are necessary for differential advection. In addition to this mechanism, small-scale horizontal winds of gravity waves directly produce layered ozone profiles [Gibson-Wilde *et al.*, 1997; Yamamori *et al.*, 2004].

[5] Vertical advection across isentropic surfaces also generates small-scale structures in ozone profiles. Holton [1987] argued that the horizontal variability of ozone mixing ratios measured from aircrafts can be attributed to the vertical advection caused by gravity waves on the basis of the phase correlation between the fluctuations of the ozone mixing ratio and potential temperature. High correlation, Holton [1987] suggested, indicates a major contribution of vertical advection as it crosses isentropic surfaces and then causes coherent fluctuations of potential temperature and the mixing ratio. In contrast, low correlation indicates a major contribution of horizontal advection, which is defined as advection along isentropic surfaces and thus does not cause fluctuations of potential temperature. Teitelbaum *et al.* [1994, 1996] examined the correlation between the small-scale structures of the ozone mixing ratio and the potential temperature in their vertical profiles, that were obtained by balloon-based measurements at 0–30 km altitudes in the northern high latitudes (60°N–80°N). These studies found that mixing ratio fluctuations were induced by vertical advection due to gravity waves in many of the ozone profiles.

[6] The latitudinal, longitudinal, and seasonal variations in the origin of small-scale layered structures need to be clarified to understand the global climatology of diffusive

transport. Pierce and Grant [1998] and Grant *et al.* [1998] investigated statistically the correlation between the vertical structures of the ozone mixing ratio and potential temperature with vertical wavelengths of ≤ 2.5 km. They concluded that the activities of both vertical and horizontal advection have maxima in winter in the midlatitudes and that vertical advection dominates throughout the year in the low latitudes. However, only one measurement station was available in the midlatitudes, and no station was available in the high latitudes in their study. Ogino *et al.* [1997] obtained the meridional distribution of correlation coefficients between the ozone mixing ratio and potential temperature over the latitude range of 43°N–62°S along the 120°E meridian using ozonesonde data acquired by a research vessel in November and December. They found higher correlations near the Equator than in the midlatitudes; however, seasonal and longitudinal variations could not be derived because of limited data coverage.

[7] The present study is the first to address the origin of layered ozone structures in the lower stratosphere over a wide longitudinal and latitudinal range for all seasons. Using data from global in situ ozone and temperature measurements, we examined structures with vertical wavelengths less than 3 km. Section 2 describes the nature of the ozonesonde data used in the analysis. Section 3 provides the meridional distributions and the seasonal variations of the mixing ratio variability, the contribution of vertical advection, the contribution of horizontal advection, and the correlation between the ozone mixing ratio and potential temperature. The contribution of vertical advection was estimated from the potential temperature fluctuation and the background mixing ratio gradient. The contribution of horizontal advection was obtained by subtracting the verti-

Table 1. List of Observation Stations^a

ID	Station	N Lat.	E Lon.	Alt., m	Data Period	Number of Profiles	Data Provider
a	Alert	82.5	-62.3	66	1997, 2000–2002	186	WOUDC
b	Sodankyla	67.4	26.7	179	1988–1998	713	WOUDC
c	Churchill	58.7	-94.1	30	2000, 2001	97	WOUDC
d	Stonyplain	53.6	-114.1	766	2000–2002	97	WOUDC
e	Goose Bay	53.2	-60.2	36	2000–2002	116	WOUDC
f	UCCLE	50.8	4.4	100	1990–2001	1709	WOUDC
g	Payerne	46.5	6.6	491	1990–2002	1755	WOUDC
h	Sapporo	43.1	141.3	19	1990–2000	422	JMA
i	Tsukuba	36.1	140.1	31	1990–2000	594	JMA
j	Huntsville	35.3	-86.6	196	1999–2002	127	WOUDC
k	Kagoshima	31.6	130.6	31	1995–2000	259	JMA
l	Santa Cruz	28.5	-16.3	36	1996, 1999, 2000–2002	297	WOUDC
m	Naha	26.2	127.7	27	1990–2000	408	JMA
n	Paramaribo	5.8	-55.2	7	1999–2002	153	WOUDC
o	San Cristobal	-0.9	-89.6	8	1998–2001	183	WOUDC
p	Nairobi	-1.3	36.8	1795	1998–2001	182	WOUDC
q	Watukosek	-7.6	112.7	50	1999–2002	112	WOUDC
r	Ascension Island	-8.0	-14.4	91	1998–2001	174	WOUDC
s	Samoa	-14.2	-170.6	77	1995–2002	303	WOUDC
t	Papeete	-18.0	-149.0	2	1995–1999	168	WOUDC
u	Suva	-18.1	178.4	6	1997–2002	205	WOUDC
v	Irene	-26.0	28.2	1524	1998–2002	112	WOUDC
w	Lauder	-45.0	169.7	370	1989–2002	880	WOUDC
x	Neumayer	-70.7	-8.2	42	1992–2003	840	WOUDC

^aID refers to plots in Figures 3–7. Lat. is latitude, Lon. is longitude, and Alt. is altitude.

cal advection component from the observed value. The origin of horizontal advection is also discussed by using assimilated meteorological data. Section 4 summarizes the conclusions.

2. Data Set

[8] The ozonesonde data used in the present study were provided by the World Ozone and Ultraviolet Radiation Data Centre (WOUDC) and the Japan Meteorological Agency (JMA). Approximately 10,000 ozonesonde profiles with high vertical resolution of $R = 10\text{--}80$ m were obtained at 24 stations spanning 82.5°N to 70.7°S , as listed in Table 1. All stations provided vertical profiles of temperature, pressure, and ozone number density, which were converted to potential temperature and the ozone mixing ratio in the analysis. The data were resampled onto a regular vertical grid at 100-m intervals because the band-pass filter used in the analysis required regularly spaced data points.

[9] The error in the ozone measurement is $\sigma \sim 3\%$ [Komhyr *et al.*, 1995] and that in the temperature measurement is $\sigma \sim 0.2$ K [Lamsal *et al.*, 2004] for electrochemical concentration cell (ECC) ozonesondes in the lower stratosphere. To lower the noise level, the structures with vertical wavelengths less than 500 m were smoothed out by applying a low-pass filter. As a result, the error was reduced to $\sigma/\sqrt{500/R} = 0.4\text{--}1\%$ for the ozone mixing ratio and $0.03\text{--}0.08$ K for temperature. In most of the filtered profiles, the observed fluctuation amplitudes were much larger than these improved noise levels.

3. Characteristics of Small-Scale Structures

3.1. Observed Small-Scale Fluctuation in the Ozone Mixing Ratio

[10] The fluctuation components of the observed ozone mixing ratio χ , denoted by $\delta\chi_{obs}$, and of the potential

temperature, $\delta\theta$, were extracted from the original profiles using a 3-km high-pass filter after applying a 500-m low-pass filter to reduce the noise level as described in section 2. An example of this procedure is given in Figures 2a and 2b. The root mean squares (RMSs) of $\delta\chi_{obs}$, denoted by $\langle\delta\chi_{obs}\rangle$, were calculated from $\delta\chi_{obs}$ at each altitude (1-km steps) in a given month throughout the measurement period at each station. These values are displayed in Figure 3 as a function of the month and altitude for all stations.

[11] The $\langle\delta\chi_{obs}\rangle$ tends to be larger above the potential temperature of 700 K (~ 27 km altitude) than below that potential temperature at most of the stations. Seasonally, $\langle\delta\chi_{obs}\rangle$ increases in winter–spring and decreases in summer–autumn in the midlatitudes and high latitudes. Near the Equator, however, seasonal variation is unclear. These results confirm earlier statistical studies on ozone laminae in the lowermost stratosphere [e.g., Reid and Vaughan, 1991].

[12] Local minima of $\langle\delta\chi_{obs}\rangle$ exist around 600 K (~ 24 km) in the winter in midlatitude and high-latitude areas of both hemispheres and descend to ~ 500 K (~ 20 km) in other seasons, especially in the Northern Hemisphere. Ehhalt *et al.* [1983] and Röth and Schmidt [1990] found that variances in tracer mixing ratios have local minima at altitudes of approximately 22 km (550 K) in March and April on the basis of balloon-borne observations of long-lived trace gases (CH_4 , N_2O , CFCl_3 , and CF_2Cl_2) in southern France (44°N) and ozone in southern Germany (48°N). The present study shows that the occurrence of such local minima in the tracer profiles is not a local but a global feature.

[13] If heterogeneous chemical reactions occur on the surfaces of polar stratospheric cloud particles, the chemical lifetime of ozone can become as short as 10 days [Cariolle *et al.*, 1990; Hofmann *et al.*, 1995]. The ozone fluctuations observed in the polar winter and spring (e.g., the increase of ozone fluctuations around 500 K in September shown in

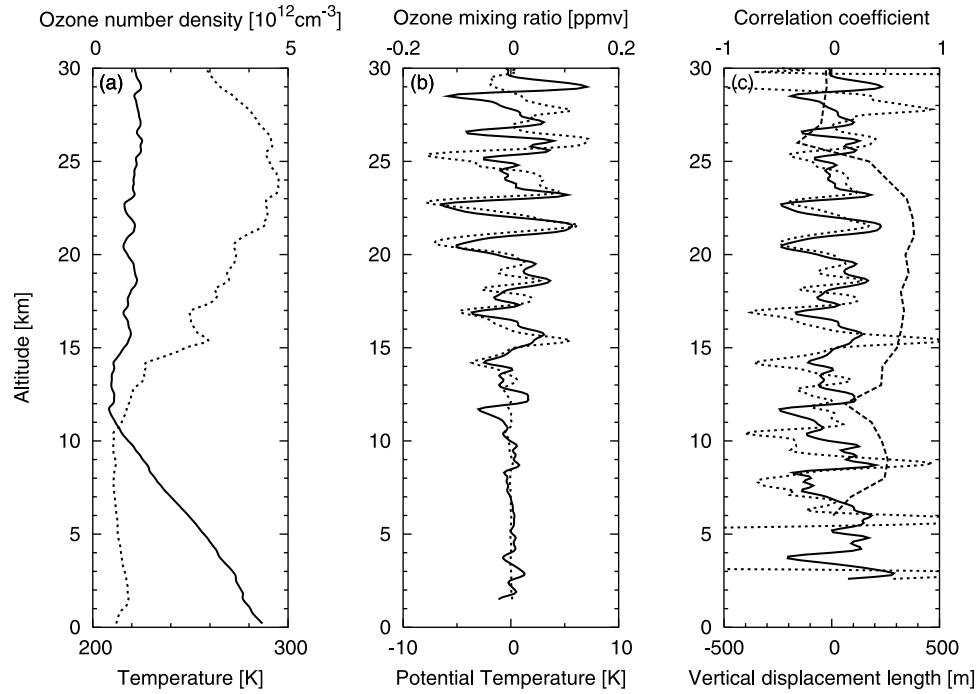


Figure 2. Example of the data processing procedure. (a) Altitude profiles of temperature (solid curve) and ozone number density (dotted curve). (b) Fluctuation components of potential temperature (solid curve) and ozone mixing ratio (dotted curve) extracted from the original profiles by a 3-km high-pass filter. (c) Vertical displacement lengths derived from potential temperature (solid curve) and ozone mixing ratio (dotted curve) and the correlation coefficient between them (dashed curve). The data were obtained at Sapporo (43.1°N, 141.3°E) on 24 November 1999.

Figure 3x) are possibly attributed to chemical processes as well as dynamical processes.

3.2. Contribution of Vertical Advection

[14] The contribution of vertical advection to the ozone mixing ratio fluctuation in each profile, $\delta\chi_v$, was estimated from the potential temperature fluctuation $\delta\theta$ as

$$\delta\chi_v = \left(\frac{\partial \bar{\chi}}{\partial z} \right) \delta Z_\theta, \quad (1)$$

where $\partial \bar{\chi} / \partial z$ is the background gradient of the ozone mixing ratio and δZ_θ is the vertical displacement length estimated as [Teitelbaum *et al.*, 1994, 1996]

$$\delta Z_\theta \equiv \delta\theta \left(\frac{\partial \bar{\theta}}{\partial z} \right)^{-1} \quad (2)$$

with $\partial \bar{\theta} / \partial z$ being the background gradient of the potential temperature. The background components (θ , $\bar{\chi}$) were calculated for each profile using a 5-km low-pass filter. The RMS of $\delta\chi_v$, denoted by $\langle \delta\chi_v \rangle$, was calculated at each altitude (1-km steps) for each station from all profiles in a given month throughout the measurement period.

[15] Figure 4 shows $\langle \delta\chi_v \rangle$ as a function of month and altitude at all stations. The $\langle \delta\chi_v \rangle$ tends to decrease above 700 K (~ 27 km) because the ozone mixing ratio approaches its peak and the vertical gradient is small in this region. Below 700 K, $\langle \delta\chi_v \rangle$ is larger in the low latitudes than in the high latitudes, because both δZ_θ and $\partial \bar{\chi} / \partial z$ are larger at

lower latitudes in the altitude region of 500 to 700 K, and δZ_θ is larger at lower latitudes below 500 K.

[16] The $\langle \delta\chi_v \rangle$ varies significantly with season with maxima in winter around 400–700 K (15–27 km) in the midlatitudes, primarily because of the winter maximum of $\langle \delta Z_\theta \rangle$. Pierce and Grant [1998] also observed a similar tendency in data collected at Wallops Island, VA (38°N, 75°E); the present study showed that such a seasonal variation occurs over wide longitudinal regions. The seasonal variation in $\langle \delta\chi_v \rangle$ may be attributable to the seasonal variation in gravity wave activity, which reaches a maximum in winter in the midlatitudes [Kitamura and Hirota, 1989; Allen and Vincent, 1995; Ogino *et al.*, 1999].

3.3. Contribution of Horizontal Advection

[17] The contribution of horizontal advection to the mixing ratio fluctuation in each profile, $\delta\chi_h$, was obtained by subtracting the contribution of vertical advection $\delta\chi_v$ from the observed value $\delta\chi_{obs}$. The RMS of $\delta\chi_h$, denoted by $\langle \delta\chi_h \rangle$, was calculated at each altitude (1-km step) of each station from all profiles in a given month throughout the measurement period.

[18] Figure 5 shows $\langle \delta\chi_h \rangle$ as a function of month and altitude. The comparison of $\langle \delta\chi_v \rangle$ (Figure 4) to $\langle \delta\chi_h \rangle$ suggests that horizontal advection is always the major source of the mixing ratio fluctuation above 700 K (~ 27 km). Below 700 K, however, the source of the mixing ratio fluctuation depends on latitude, as described below. Horizontal advection governs the mixing ratio fluctuation at high latitudes (50°N–90°N and 50°S–90°S), while vertical advection

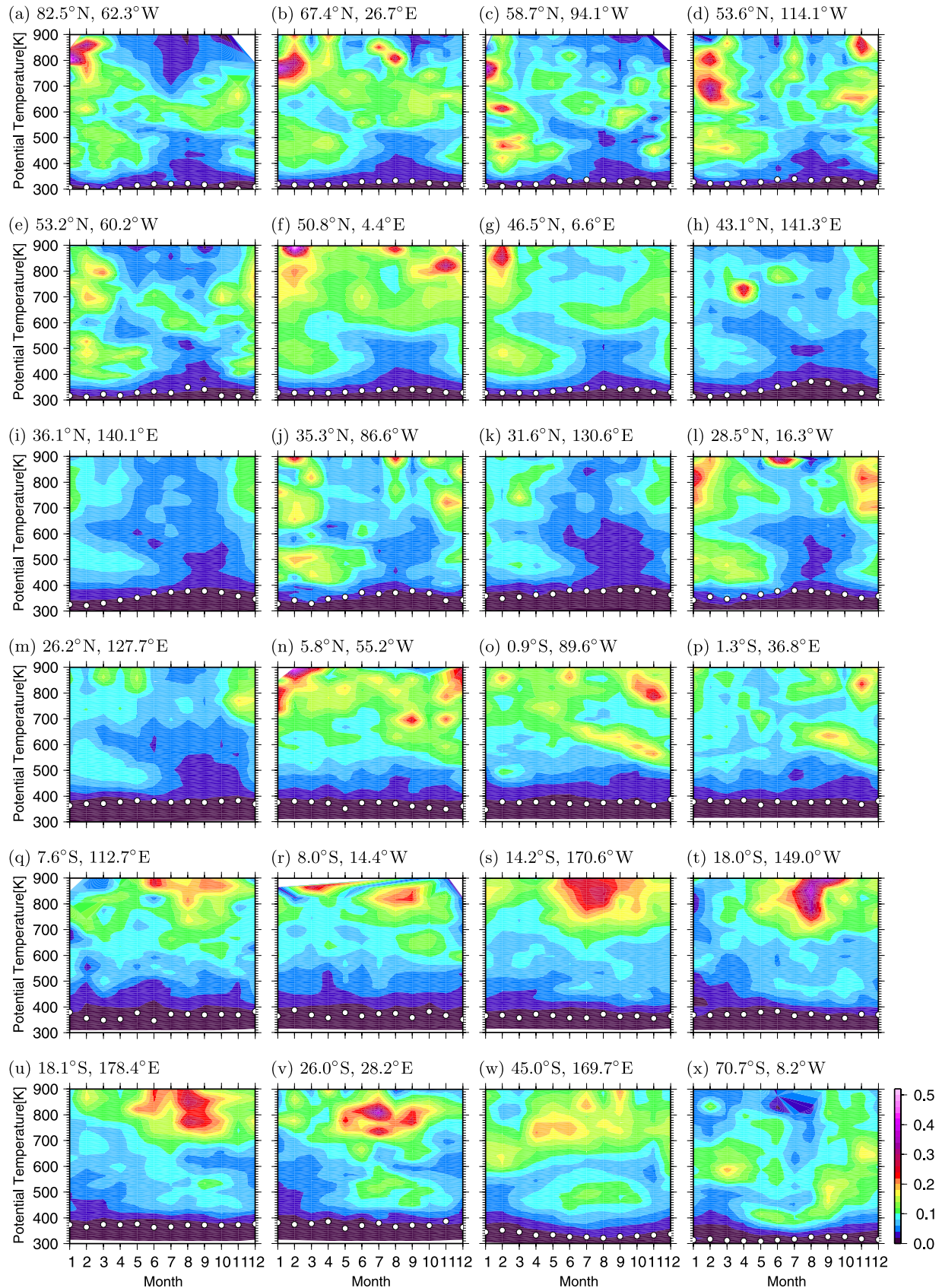


Figure 3. Seasonal and altitudinal dependence of the RMS of small-scale fluctuation in the ozone mixing ratio observed by ozonesondes, in units of ppmv. White circles indicate tropopause altitudes.

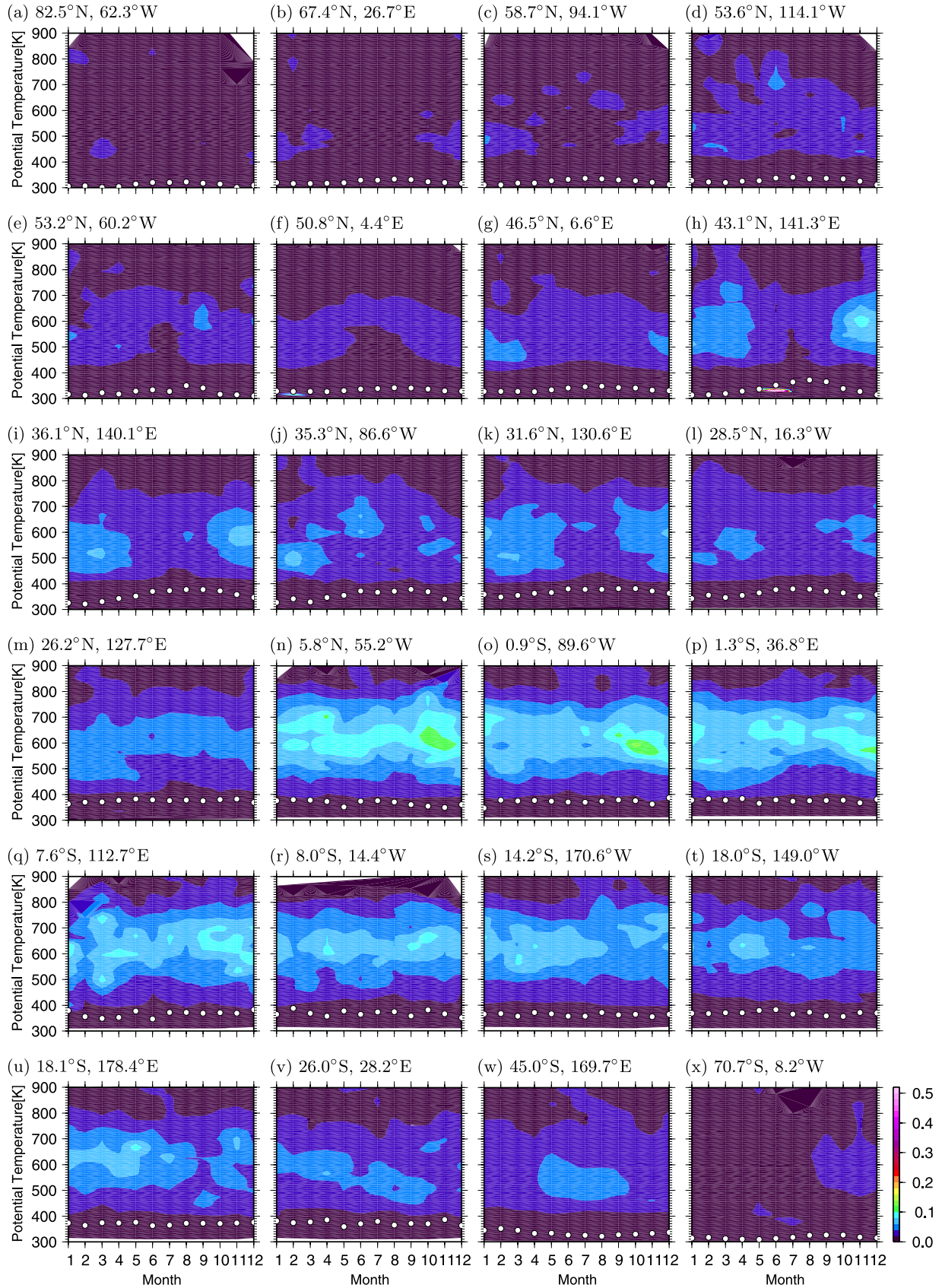


Figure 4. Same as Figure 3, but for the RMS of the small-scale mixing ratio fluctuation induced by vertical advection.

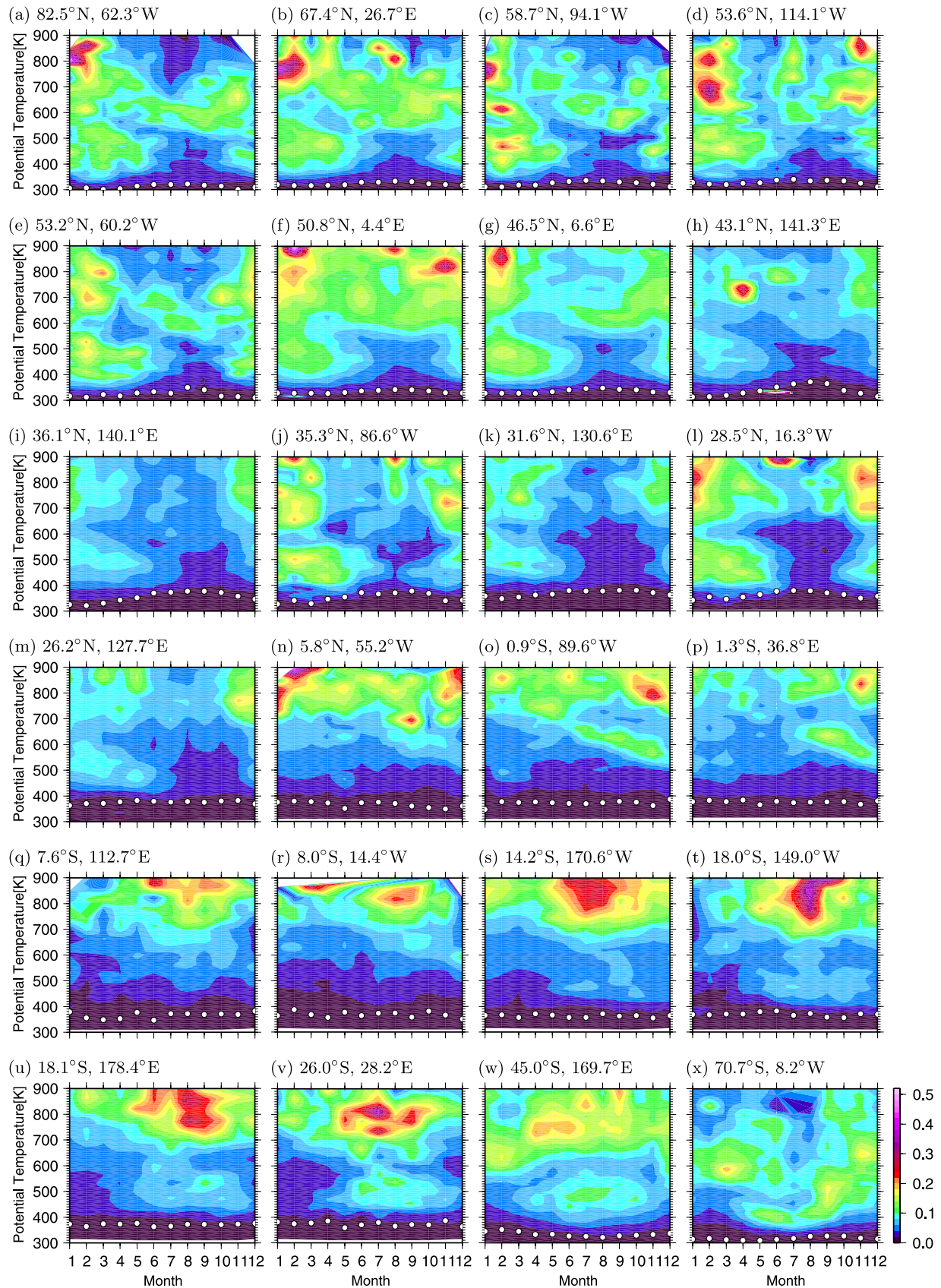


Figure 5. Same as Figure 3, but for the RMS of the small-scale mixing ratio fluctuation induced by horizontal advection.

dominates at low latitudes (20°S–20°N). In the midlatitudes (20°N–50°N and 20°S–50°S), the contributions of horizontal advection and vertical advection show qualitatively similar seasonal variation with maxima in winter–spring. However, the seasonal variation of horizontal advection is much larger than that of vertical advection; as a result, horizontal advection dominates in winter–spring and vertical advection dominates in summer–autumn. The factors that determine the activity of horizontal advection are discussed in section 3.5.

3.4. Correlation Between the Mixing Ratio and Potential Temperature

[19] To clarify the regions where vertical advection dominates, we examined the correlations between the fluctuations in the ozone mixing ratio and potential temperature. Instead of directly calculating the correlation coefficient, the correlation coefficient between the vertical displacement δZ_θ defined by equation (2) and δZ_χ defined by [Teitelbaum *et al.*, 1994, 1996]

$$\delta Z_\chi \equiv \delta\chi \left(\frac{\partial \bar{\chi}}{\partial z} \right)^{-1} \quad (3)$$

was calculated for each altitude (1-km steps) from the data within the nearest ± 3 km (60 points) in each profile. These correlation coefficient profiles were monthly averaged at each station. Figure 2c shows typical profiles of δZ_θ and δZ_χ together with the correlation coefficient between them. High correlations are found at 14–25 km altitudes, indicating that vertical advection is responsible for the mixing ratio fluctuation in this region. In other altitude regions, horizontal advection is supposed to be responsible for the mixing ratio fluctuation.

[20] The resultant correlation coefficients are shown as a function of season and altitude in Figure 6. It is clear from Figure 6 that high correlation coefficients are found in regions where vertical advection is dominant according to the results in section 3.3, i.e., the low latitudes and in the midlatitudes in summer–autumn. The structures around the tropopause may have resulted from the sharp curvature in the temperature and ozone profiles in this region; hereafter, we do not discuss these structures.

[21] The increase in the correlation coefficients toward the Equator is consistent with the previous results which are based on observations at limited longitudes [Grant *et al.*, 1998; Pierce and Grant, 1998; Ogino *et al.*, 1997]. Although some longitude dependences are evident from the comparisons of Figures 6d and 6e, 6i and 6j, 6o and 6p, 6q and 6r, and 6t and 6u, it is less prominent than the latitude dependence. This suggests that the magnitude of vertical advection relative to horizontal advection principally depends on the latitude and tends to be zonally symmetric.

3.5. Horizontal Advection Derived From Meteorological Data

[22] To examine the factors controlling the horizontal advection activity, we compared the horizontal advection component estimated from observations (Figure 5) with the horizontal advection activity due to synoptic-scale motions which are reproduced in the National Centers for Environmental Prediction/National Center for Atmospheric Re-

search (NCEP/NCAR) reanalysis data [Kalnay *et al.*, 1996]. Although the vertical wavelengths resolved by the NCEP/NCAR reanalysis data in the lower stratosphere (≥ 4 –6 km) are larger than those examined in this paper (≤ 3 km), the observed basic features can be reproduced from the coarse NCEP/NCAR data if differential advection due to large-scale horizontal winds (see section 1) is responsible for the small-scale fluctuations of the mixing ratio [Newman and Schoeberl, 1995; Orsolini *et al.*, 1995; Schoeberl and Newman, 1995].

[23] Assuming that the mixing ratio fluctuation was caused by the meridional displacement of air parcels on isentropic surfaces, the RMS of the synthetic mixing ratio fluctuation $\langle \delta\chi_{synth} \rangle$ was estimated as

$$\langle \delta\chi_{synth} \rangle = \frac{\partial \bar{\chi}}{\partial y} \langle \delta y \rangle, \quad (4)$$

where y is the northward coordinate, $\partial \bar{\chi} / \partial y$ is the zonal mean meridional gradient of the ozone mixing ratio taken from URAP data (Figure 1), and $\langle \delta y \rangle$ is the RMS of the meridional displacement length. The $\langle \delta y \rangle$ was estimated from NCEP/NCAR reanalysis data as follows:

$$\langle \delta y \rangle = \langle \delta\zeta \rangle \left(\frac{\partial \bar{\zeta}}{\partial y} \right)^{-1}, \quad (5)$$

where $\langle \delta\zeta \rangle$ is the RMS of the potential vorticity fluctuation with periods less than 10 days at each altitude, and $\partial \bar{\zeta} / \partial y$ is the zonal mean meridional gradient of potential vorticity. Synoptic-scale transient eddies were extracted by a 10-day high-pass filter. The y derivatives in equations (4) and (5) were calculated on isentropic surfaces.

[24] Although $\langle \delta\chi_{synth} \rangle$ is simply a measure of large-scale advection and is not necessarily the amplitude of small-vertical-scale structures, it is expected to have a behavior qualitatively similar to that of small-vertical-scale structures caused by differential advection. Large-scale horizontal advection caused by the breaking of planetary waves and/or the erosion of polar vortex would bring about filamentary horizontal structures of tracers if there were background horizontal gradients in the tracer mixing ratios. Once filamentary structures of ozone are generated through such processes, small-vertical-scale structures would be created via large-scale horizontal winds accompanied by vertical shear (see section 1).

[25] Figure 7 shows the calculated $\langle \delta\chi_{synth} \rangle$ as a function of month and altitude. The basic features of the horizontal advection component estimated from observations (Figure 5) are reproduced in Figure 7: $\langle \delta\chi_{synth} \rangle$ tends to be larger above 700 K (~ 27 km) than below, $\langle \delta\chi_{synth} \rangle$ increases in winter–spring and decreases in summer–autumn in the middle and high latitudes, and local minima exist around 600 K (~ 24 km) in the winter in middle and high latitudes and descend to ~ 500 K in other seasons. This suggests that the seasonal behavior and the latitudinal/altitudinal tendencies of small-scale vertical structures can be reproduced by the combination of NCEP/NCAR reanalysis and URAP data and that large-scale horizontal advection has a major contribution to the generation of the observed mixing ratio fluctuations.

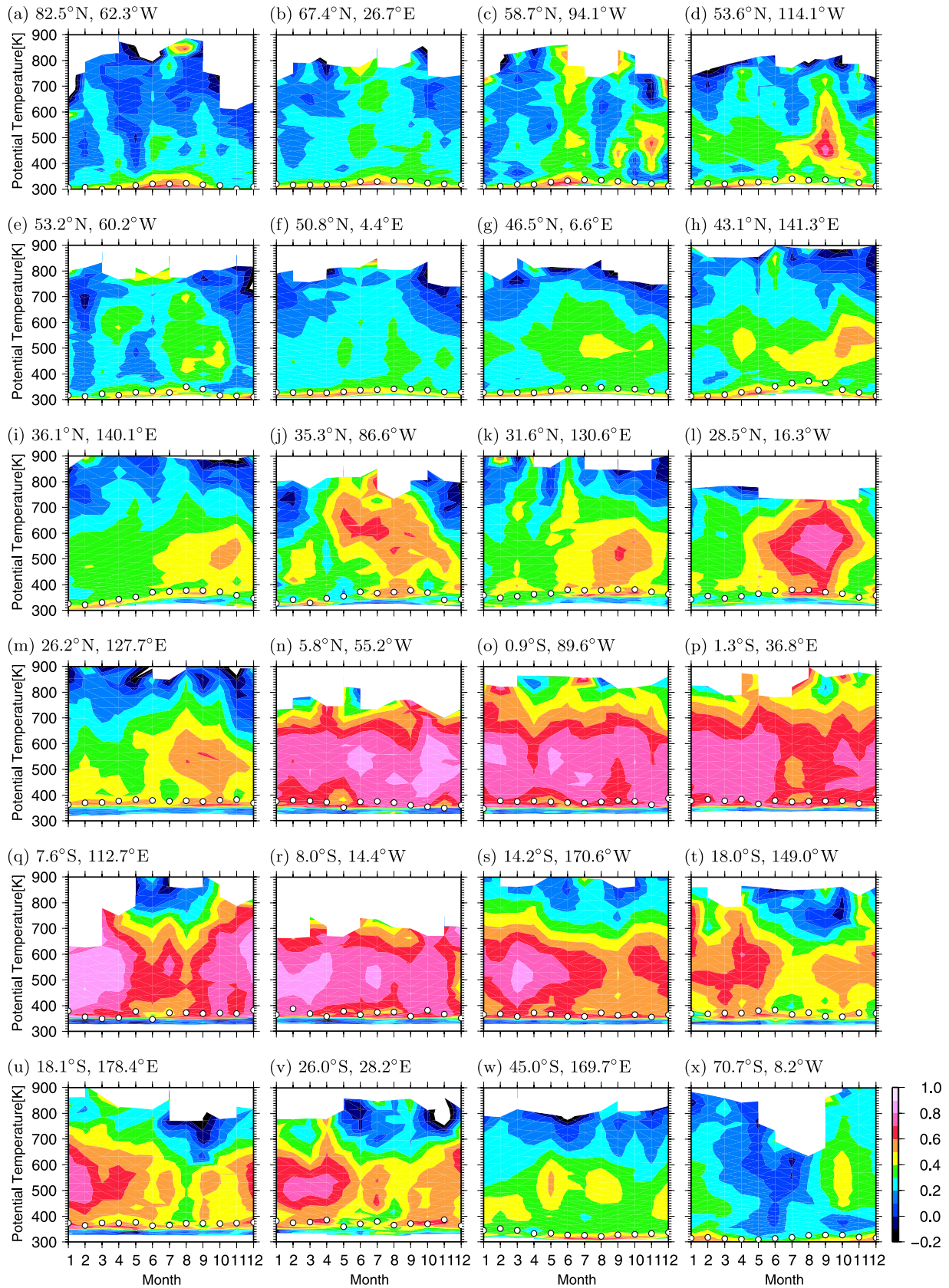


Figure 6. Same as Figure 3, but for the correlation coefficient between the vertical displacement length derived from ozone mixing ratio and that derived from potential temperature.

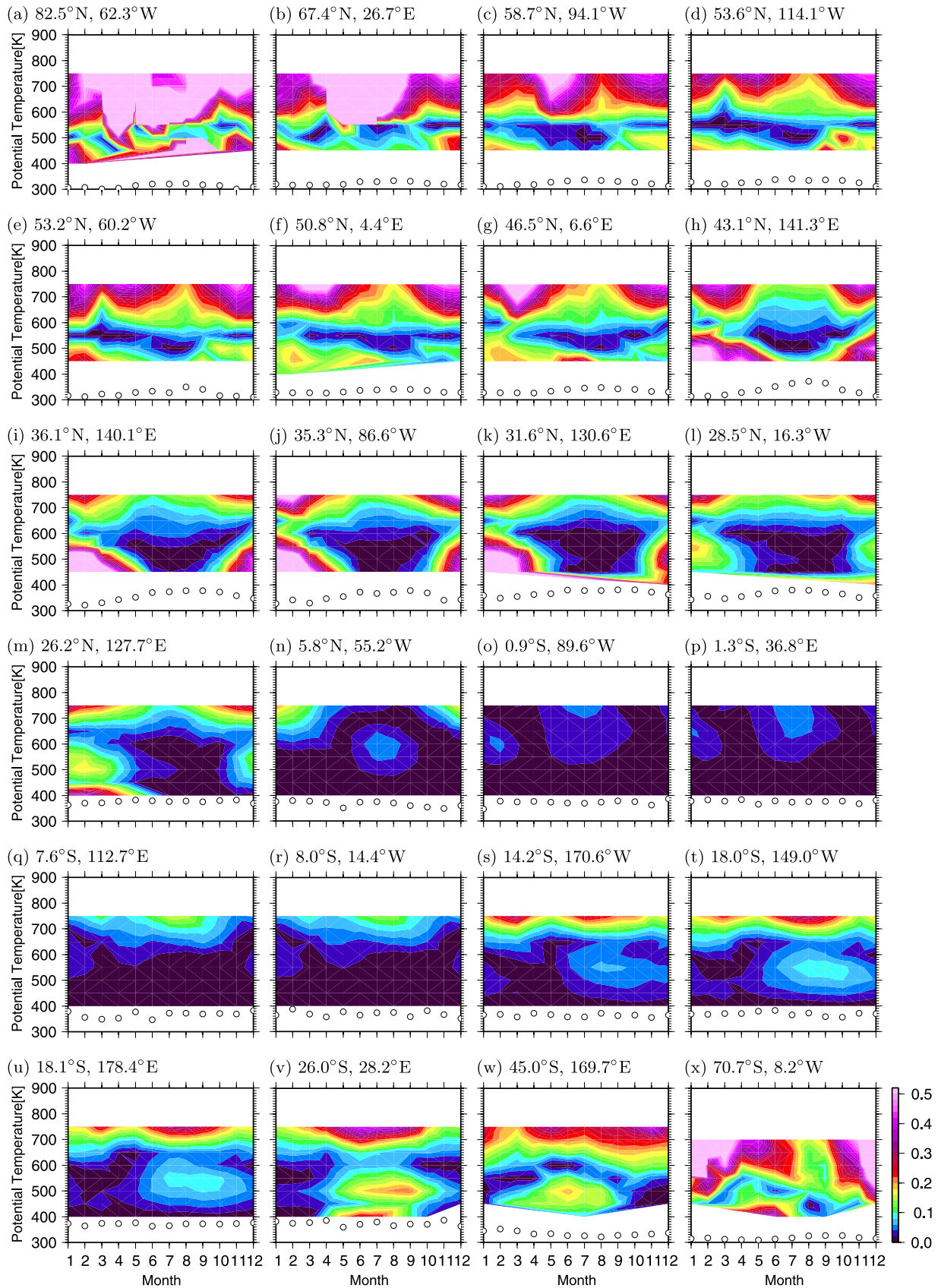


Figure 7. Same as Figure 3, but for the RMS of the synthetic mixing ratio fluctuation caused by synoptic-scale horizontal winds, which were calculated from assimilated meteorological data and the mean meridional distribution of the mixing ratio (see text).

[26] The distribution and seasonal variations of $\langle \delta\chi_{synth} \rangle$ are primarily determined by those of $\partial\bar{\chi}/\partial y$ (data not shown), suggesting tentatively that the horizontal advection component estimated from observations (Figure 5) is also controlled by $\partial\bar{\chi}/\partial y$. The local minima of $\langle \delta\chi_h \rangle$ at 600 K (~ 24 km) are attributable to the smallness of $\partial\bar{\chi}/\partial y$ in this region; $\partial\bar{\chi}/\partial y$ changes its sign around 600 K from positive (negative) at lower altitudes to negative (positive) at higher altitudes in the Northern (Southern) Hemisphere (Figure 1). *Ehhalt et al.* [1983] and *Röth and Schmidt* [1990] ascribed such minima in the mixing ratio variances around 22 km in altitude (see section 3.1) to the weakening of the dynamical activity causing the advection of tracers. However, at least for ozone, the present results suggest that the lack of the meridional gradient in the mixing ratio is responsible for the local minima rather than the weakening of dynamical activity.

3.6. Contribution of Gravity Waves to Horizontal Advection

[27] Small-scale horizontal winds associated with gravity waves may also contribute to the mixing ratio fluctuation, although gravity waves were considered as the process causing vertical advection in section 3.2. Under the assumption that the long axes of gravity waves are aligned north-south, the maximal magnitude of the ozone mixing ratio fluctuation caused by the horizontal winds of gravity waves can be estimated by multiplying the horizontal displacement lengths by the mean meridional gradient of the mixing ratio. Typical gravity waves in the stratosphere have intrinsic periods of $T = 2\pi/3f - 2\pi/f$ and horizontal wind amplitudes of $|v'| \sim 5 \text{ m s}^{-1}$ in the midlatitudes and high latitudes [e.g., *Sato, 1994; Vincent et al., 1997*], while they have $T = 20\text{--}80$ hours and $|v'| \sim 5 \text{ m s}^{-1}$ in the low latitudes [e.g., *Tsuda et al., 1994; Ogino et al., 1995; Sato et al., 2003*], where f is the Coriolis parameter. Letting $T = 2\pi/2f$ in the midlatitudes and high latitudes and $T = 50$ hours in the low latitudes, and $|v'| = 5 \text{ m s}^{-1}$, mixing ratio fluctuations are estimated to be less than $\sim 20\%$ and $\sim 50\%$ below and above 600 K (~ 24 km), respectively. This estimation suggests that small-scale horizontal advection caused by gravity waves possibly makes a nonnegligible contribution, although the contribution does not seem to exceed the contribution of differential advection via large-scale horizontal winds.

4. Conclusions

[28] This study investigated the origin of small-vertical-scale (wavelength 0.5–3 km) fluctuations of the ozone mixing ratio in the lower stratosphere over a broad longitudinal and latitudinal region for all seasons using data obtained by ozonesondes launched at 24 stations spanning 82.5°N to 70.7°S. The meridional distribution and seasonal variation of the mixing ratio variability, its vertical advection component, and its horizontal advection component were obtained from the data set. The vertical advection component was estimated from the potential temperature fluctuation and the mean vertical gradient of the mixing ratio. The horizontal advection component was obtained by subtracting the vertical advection component from the observed mixing ratio fluctuation.

[29] Horizontal advection is always the major source of the mixing ratio fluctuation above 700 K (~ 27 km). The contribution of vertical advection is small in this region because the vertical gradient of the mixing ratio is small. Below 700 K the source of the fluctuation depends on the latitude: horizontal advection governs the mixing ratio fluctuation in the high latitudes, while vertical advection is dominant in the low latitudes. In the midlatitudes, although horizontal and vertical advection contributions show qualitatively similar seasonal variations with maxima in winter–spring, horizontal advection is relatively dominant in winter–spring and vertical advection is dominant in summer–autumn. This tendency was also confirmed by analyzing the correlation coefficients between small-scale structures of the mixing ratio and the potential temperature. Local minima of mixing ratio variability that are found at approximately 600 K (~ 24 km) in the winter in midlatitudes and high latitudes are attributable to the absence of the latitudinal gradient in the mixing ratio in this season, which creates inefficient horizontal advection.

[30] Extended studies are needed to evaluate the extent to which these small-scale structures lead to irreversible diffusive transport. Studies that estimate the diffusion coefficients by other methods combined with the observation of small-scale mixing ratio structures should be conducted. *Legras et al.* [2003] estimated the vertical diffusion coefficients by comparing the ozone laminae observed by ozonesondes and ozone profiles reconstructed from backward trajectory calculations, assuming that the observed profiles were smeared by vertical diffusion compared to the reconstructed profiles. More comprehensive analysis can be achieved by applying this method to global ozonesonde data and comparing the resultant diffusivity distribution to the distribution of horizontal advection and vertical advection revealed in the present study.

[31] **Acknowledgments.** We are grateful to N. Iwagami, M. Koike, H. Nakamura, and M. Takahashi for valuable comments on earlier drafts of this manuscript. We also thank S. Hayashida for detailed comments and suggestions that greatly improved the paper. The global ozonesonde data were supplied by the World Ozone and Ultraviolet Radiation Data Centre through their Web site (<http://www.woudc.org/>) and the Japan Meteorological Agency. The NCEP reanalysis data were provided by the NOAA-Cooperative Institute for Research in Environmental Sciences (CIRES) Climate Diagnostics Center, Boulder, Colorado, through their Web site (<http://www.cdc.noaa.gov/>). The zonal mean ozone data were provided by the UARS Reference Atmosphere Project through their Web site (<http://code916.gsfc.nasa.gov/Public/Analysis/UARS/urap/home.html>).

References

- Allen, S. J., and R. A. Vincent (1995), Gravity wave activity in the lower atmosphere: Seasonal and latitudinal variations, *J. Geophys. Res.*, **100**, 1327–1350.
- Brasseur, G., and S. Solomon (1986), *Aeronomy of the Middle Atmosphere*, 2nd ed., 452 pp., Springer, New York.
- Cariolle, D., A. Lasserre-Bigorry, J.-F. Royer, and J.-F. Geleyn (1990), A general circulation model simulation of the springtime Antarctic ozone decrease and its impact on midlatitudes, *J. Geophys. Res.*, **95**, 1883–1898.
- Ehhalt, D. H., E. P. Röth, and U. Schmidt (1983), On the temporal variance of stratospheric trace gas concentrations, *J. Atmos. Chem.*, **1**, 27–51.
- Fukao, S., M. D. Yamanaka, N. Ao, W. K. Hocking, T. Sato, M. Yamamoto, T. Nakamura, T. Tsuda, and S. Kato (1994), Seasonal variability of vertical eddy diffusivity in the middle atmosphere: 1. Three-year observations by the middle and upper atmosphere radar, *J. Geophys. Res.*, **99**, 18,973–18,988.
- Gibson-Wilde, D. E., R. A. Vincent, C. Souprayen, S. Godin, A. Hertzog, and S. D. Eckermann (1997), Dual lidar observations of mesoscale

- fluctuations of ozone and horizontal winds, *Geophys. Res. Lett.*, **24**, 1627–1630.
- Grant, W. B., R. B. Pierce, S. J. Oltmans, and E. V. Browell (1998), Seasonal evolution of total and gravity wave induced laminae in ozonesonde data in the tropics and subtropics, *Geophys. Res. Lett.*, **25**, 1863–1866.
- Hofmann, D. J., S. J. Oltmans, B. J. Johnson, J. A. Lathrop, J. M. Harris, and H. Vomel (1995), Recovery of ozone in the lower stratosphere at the South Pole during the spring of 1994, *Geophys. Res. Lett.*, **22**, 2493–2496.
- Holton, J. R. (1987), The production of temporal variability in trace constituent concentrations, in *Transport Process in the Middle Atmosphere*, edited by G. Visconti and R. Garcia, pp. 313–326, Springer, New York.
- Holton, J. R., P. H. Haynes, M. E. McIntyre, A. R. Douglass, R. B. Rood, and L. Pfister (1995), Stratosphere-troposphere exchange, *Rev. Geophys.*, **33**, 403–439.
- Juckes, M. N., and M. E. McIntyre (1987), A high-resolution one-layer model of breaking planetary waves in the stratosphere, *Nature*, **328**, 590–596.
- Kalnay, E., et al. (1996), The NCEP/NCAR 40-year reanalysis project, *Bull. Am. Meteorol. Soc.*, **77**, 437–471.
- Kitamura, Y., and I. Hirota (1989), Small-scale disturbances in the lower stratosphere revealed by daily rawin sonde observations, *J. Meteorol. Soc. Jpn.*, **67**, 817–830.
- Komhyr, W. D., R. A. Barnes, G. B. Brothers, J. A. Lathrop, and D. P. Opperman (1995), Electrochemical concentration cell ozonesonde performance evaluation during STOIC 1989, *J. Geophys. Res.*, **100**, 9231–9244.
- Lamsal, L. N., M. Weber, S. Tellmann, and J. P. Burrows (2004), Ozone column classified climatology of ozone and temperature profiles based on ozonesonde and satellite data, *J. Geophys. Res.*, **109**(D20), D20304, doi:10.1029/2004JD004680.
- Legras, B., B. Joseph, and F. Lefèvre (2003), Vertical diffusivity in the lower stratosphere from Lagrangian back-trajectory reconstructions of ozone profiles, *J. Geophys. Res.*, **108**(D18), 4562, doi:10.1029/2002JD003045.
- Lyjak, L. V., and V. A. Yudin (2005), Diagnostics of the large-scale mixing properties from stratospheric analyses, *J. Geophys. Res.*, **110**, D17107, doi:10.1029/2004JD005577.
- McIntyre, M. E., and T. N. Palmer (1983), Breaking planetary waves in the stratosphere, *Nature*, **305**, 593–600.
- Newman, P. A., and M. R. Schoeberl (1995), A reinterpretation of the data from the NASA stratosphere-troposphere exchange project, *Geophys. Res. Lett.*, **22**, 2501–2504.
- Ogino, S.-Y., M. D. Yamanaka, and S. Fukao (1995), Meridional variation of lower stratospheric gravity wave activity: A quick look at Hakuohmaru J-COARE cruise rawinsonde data, *J. Meteorol. Soc. Jpn.*, **73**, 407–413.
- Ogino, S.-Y., M. D. Yamanaka, S. Kaneto, T. Yamanouchi, and S. Fukao (1997), Meridional distribution of short-vertical-scale fluctuations in the lower stratosphere revealed by cross-equatorial ozonesonde observations on “Shirase,” *Proc. NIPR Symp. Polar Meteorol. Glaciol.*, **11**, 199–210.
- Ogino, S.-Y., M. D. Yamanaka, and S. Fukao (1999), Interannual and day-to-day variations of gravity wave activity in the lower stratosphere over the eastern part of Japan observed in winter 1989–95, *J. Meteorol. Soc. Jpn.*, **77**, 413–429.
- Orsolini, Y., P. Simon, and D. Cariolle (1995), Filamentation and layering of an idealized tracer by observed winds in the lower stratosphere, *Geophys. Res. Lett.*, **22**, 839–842.
- Pierce, R. B., and W. B. Grant (1998), Seasonal evolution of Rossby and gravity wave induced laminae in ozonesonde data obtained from Wallops Island, Virginia, *Geophys. Res. Lett.*, **25**, 1859–1862.
- Plumb, R. A., D. W. Waugh, R. J. Atkinson, P. A. Newman, L. R. Lait, M. R. Schoeberl, E. V. Browell, A. J. Simmons, and M. Loewenstein (1994), Intrusions into the lower stratospheric Arctic vortex during the winter of 1991–1992, *J. Geophys. Res.*, **99**, 1089–1106.
- Portafaix, T., B. Morel, H. Bencherif, S. Baldy, S. Godin-Beekmann, and A. Hauchecorne (2003), Fine-scale study of a thick stratospheric ozone lamina at the edge of the southern subtropical barrier, *J. Geophys. Res.*, **108**(D6), 4196, doi:10.1029/2002JD002741.
- Reid, S. J., and G. Vaughan (1991), Lamination in ozone profiles in the lower stratosphere, *Q. J. R. Meteorol. Soc.*, **117**, 825–844.
- Röth, E. P., and U. Schmidt (1990), Seasonal variation of the temporal variance of long-lived trace gases measured during MAP, *Adv. Space Res.*, **10**(10), 167–170.
- Sato, K. (1994), A statistical study of the structure, saturation and sources of inertio-gravity waves in the lower stratosphere observed with the MU rader, *J. Atmos. Terr. Phys.*, **56**, 755–774.
- Sato, K., M. Yamamori, S.-Y. Ogino, N. Takahashi, Y. Tomikawa, and T. Yamanouchi (2003), A meridional scan of the stratospheric gravity wave field over the ocean in 2001 (MeSSO2001), *J. Geophys. Res.*, **108**(D16), 4491, doi:10.1029/2002JD003219.
- Schoeberl, M. R., and P. A. Newman (1995), A multiple-level trajectory analysis of vortex filaments, *J. Geophys. Res.*, **100**, 25,801–25,815.
- Swinbank, R., and D. A. Orland (2003), Compilation of wind data for the Upper Atmosphere Research Satellite (UARS) Reference Atmosphere Project, *J. Geophys. Res.*, **108**(D19), 4615, doi:10.1029/2002JD003135.
- Teitelbaum, H., J. Ovarlez, H. Kelder, and F. Lott (1994), Some observations of gravity-wave-induced structure in ozone and water vapor during EASOE, *Geophys. Res. Lett.*, **21**, 1483–1486.
- Teitelbaum, H., M. Moustouai, J. Ovarlez, and H. Kelder (1996), The role of atmospheric waves in the laminated structure of ozone profiles at high latitude, *Tellus, Ser. A*, **48**, 442–455.
- Tomikawa, Y., K. Sato, K. Kita, M. Fujiwara, M. Yamamori, and T. Sano (2002), Formation of an ozone lamina due to differential advection revealed by intensive observations, *J. Geophys. Res.*, **107**(D10), 4092, doi:10.1029/2001JD000386.
- Tsuda, T., Y. Murayama, H. Wiryosumarto, S. W. B. Harijono, and S. Kato (1994), Radiosonde observations of equatorial atmosphere dynamics over Indonesia: 2. Characteristics of gravity waves, *J. Geophys. Res.*, **99**, 10,507–10,516.
- Vincent, R. A., S. J. Allen, and S. D. Eckermann (1997), Gravity-wave parameters in the lower stratosphere, in *Gravity Wave Processes: Their Parameterization in Global Climate Models*, NATO ASI Ser. I, vol. 50, edited by K. Hamilton, pp. 7–25, Springer, New York.
- Waugh, D. W., et al. (1994), Transport out of the lower stratospheric Arctic vortex by Rossby wave breaking, *J. Geophys. Res.*, **99**, 1071–1088.
- Yamamori, M., Y. Murayama, K. Shibasaki, and I. Murata (2004), Variations in ozone and dynamical variables in the upper troposphere and lower stratosphere as revealed in the intensive ozonesonde observation at Fairbanks, Alaska, in August 2003, paper presented at Quadrennial Ozone Symposium 2004, Int. Ozone Comm., Kos, Greece. (Available at <http://www.qos2004.gr/files/193.pdf>)

G. E. Bodeker, National Institute of Water and Atmospheric Research, Private Bag 50061, Omakau 9352, New Zealand.

T. Imamura and K.-I. Oyama, Institute of Space and Astronautical Science, Japan Aerospace Exploration Agency, 3-1-1, Yoshinodai, Sagami-hara, Kanagawa 229-8510, Japan.

K. Noguchi, Faculty of Science, Nara Women's University, Kita-uoya Nishi-machi, Nara 630-8506, Japan. (nogu@ics.nara-wu.ac.jp)